CSPS | jpps Journal of Pharmacy and Pharmaceutical Sciences

TYPE Original Research
PUBLISHED 02 November 2026
DOI 10.3389/jpps.2026.17204

Check for updates

OPEN ACCESS

EDITED BY
Fakhreddin Jamali,
University of Alberta, Canada

*CORRESPONDENCE
Xiongbiao Chen,
xbc719@mail.usask.ca
Michael E. Kelly,
m.kelly@usask.ca
Ildiko Badea,
ildiko.badea@usask.ca

RECEIVED 23 June 2026
REVISED 19 August 2026
ACCEPTED 20 October 2026
PUBLISHED 02 November 2026

CITATION
Ketabat F, Kim A, Alizadeh Sardroud H, Eames BF, Collins M, Chen X, Kelly ME and Badea I (2026) 3D bioprinting of vascularized cardiac constructs reveals improved cardiomyocyte organization and contractile function.
J. Pharm. Pharm. Sci. 29:17204.
doi: 10.3389/jpps.2026.17204

COPYRIGHT
© 2026 Ketabat, Kim, Alizadeh Sardroud, Eames, Collins, Chen, Kelly and Badea. This is an open-access article distributed under the terms of the Creative Commons Attribution License (CC BY). The use, distribution or reproduction in other forums is permitted, provided the original author(s) and the copyright owner(s) are credited and that the original publication in this journal is cited, in accordance with accepted academic practice. No use, distribution or reproduction is permitted which does not comply with these terms.

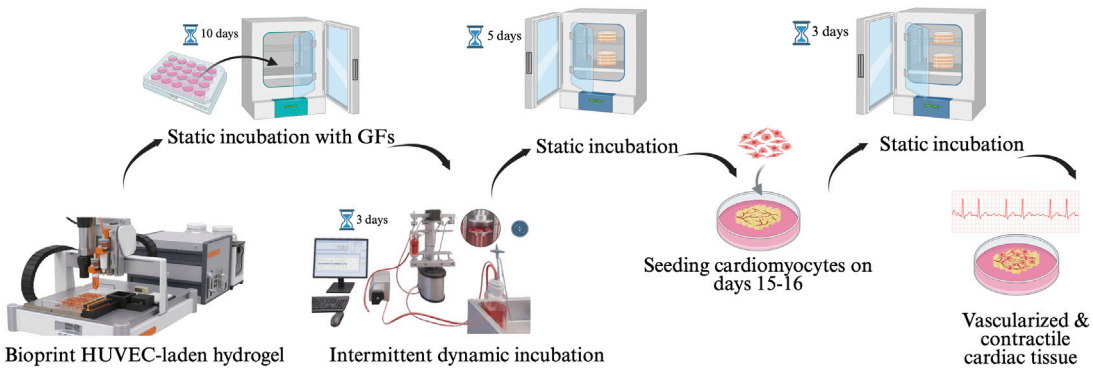
3D bioprinting of vascularized cardiac constructs reveals improved cardiomyocyte organization and contractile function

Farinaz Ketabat[1], Andy Kim[2], Hamed Alizadeh Sardroud[3], Brian Frank Eames[2], Michelle Collins[2], Xiongbiao Chen[1,4]*, Michael E. Kelly[5]* and Ildiko Badea[6]*

[1]Division of Biomedical Engineering, University of Saskatchewan, Saskatoon, SK, Canada, [2]Department of Anatomy, Physiology, and Pharmacology, University of Saskatchewan, Saskatoon, SK, Canada, [3]Department of Biosystems Engineering, Faculty of Agricultural and Food Sciences, University of Manitoba, Winnipeg, MB, Canada, [4]Department of Mechanical Engineering, University of Saskatchewan, Saskatoon, SK, Canada, [5]Department of Surgery, College of Medicine, University of Saskatchewan, Saskatoon, SK, Canada, [6]College of Pharmacy and Nutrition, University of Saskatchewan, Saskatoon, SK, Canada

Background: Despite advances in cardiac tissue engineering, generating constructs that simultaneously achieve vascularization and organized cardiomyocyte function remains a major challenge.
Methods: In this study, three-dimensional (3D) bioprinting was used to fabricate human umbilical vein endothelial cell (HUVEC)-laden alginate/gelatin constructs with defined architectures designed to mimic myocardial alignment. Constructs were cultured with vascular endothelial growth factor (VEGF) and basic fibroblast growth factor (bFGF) under static conditions followed by short-term dynamic stimulation in a bioreactor. Cardiomyocytes - H9c2 cells, neonatal rat ventricular myocytes (NRVMs), or human induced pluripotent stem cell–derived cardiomyocytes (iPSC-CMs) - were subsequently seeded onto the constructs. Vascularization and the distribution of cells were assessed using immunofluorescence, and functional activity of cardiomyocytes was evaluated by calcium transient imaging.
Results: Bioprinted constructs developed interconnected CD31-positive endothelial networks in response to growth factor supplementation and dynamic culture, whereas control constructs cultured without growth factors or bioreactor exposure showed limited vascular organization. Cardiomyocytes seeded onto vascularized constructs exhibited improved structural organization, including increased alignment and integration with endothelial networks. Functional assessment revealed more synchronized and rhythmic calcium transients compared to non-vascularized constructs.
Conclusion: This study demonstrates that combining 3D bioprinting with controlled architectural design and endothelial network formation enhances cardiomyocyte organization and function. These findings highlight the critical role of vascular-like networks in improving the performance of engineered cardiac tissues.

KEYWORDS
3D bioprinting, bioreactor, cardiac tissue engineering (CTE), contractility, vascularization



GRAPHICAL ABSTRACT

Highlights

- Helical myofibril-aligned constructs mimic native cardiac architecture.
- HUVEC bioprinting enables endothelial network formation.
- Vascularization enhances cardiomyocyte alignment and cTnT-positive area.
- Dynamic culture improves synchronized contractile behavior.
- Bioprinted constructs integrate vascularization and contractility.

Introduction

Cardiac tissue engineering (CTE) is a promising approach to address complications associated with cardiovascular disease (CVD). While conventional treatments, such as the use of left ventricular assist devices (LVADs), have become standard for patients with advanced heart failure and are associated with significant reverse remodeling at structural, cellular, and molecular levels, significant limitations still exist. One major concern is the uncertainty surrounding the long-term progression of heart failure following LVAD explantation [1, 2]. In contrast, CTE holds substantial promise for the future, particularly in end-stage heart failure, where heart transplantation remains the only definitive treatment, an option severely limited by the scarcity of donor hearts [3]. In CTE, rebuilding left ventricle or developing constructs with left ventricle-function, as a primary step, has drawn considerable attention.

The left ventricle, with the thickest myocardium, generates the contractile forces necessary for systemic circulation [4]. Consequently, most research focuses on rebuilding the left ventricle as a primary step in cardiac tissue engineering. Therefore, understanding the 3D structure of the left ventricle is vital. Notably, the myocardial fibres in the left ventricle exhibit a unique helical alignment that gradually transitions from the epicardium (−70°) to the endocardium (+80°), causing them to contract in opposite directions and contributing to the left ventricular twist. This coordinated contraction enhances effective blood circulation [4, 5]. However, such helical or orientated fibres pose significant challenges in CTE. Among various methods, three-dimensional (3D) bioprinting has attracted significant attention as a potential solution to develop constructs for CTE. This technique offers the opportunity to reconstruct the complex 3D architecture of the myocardium or even the entire heart by depositing cells and biomaterials layer by layer in 3D space using a robotic arm [6].

3D bioprinting for functional CTE constructs, though promising, is still unachievable today. One major obstacle is to create vascular networks within engineered cardiac constructs. Such vascular networks are essential to ensure adequate perfusion of oxygen and nutrients throughout the entire structure for supporting the development of fully viable and functional cell-laden constructs [7, 8]. A promising approach is the combination of 3D bioprinting of vessel structures with the induction of microcapillary branching through the introduction of angiogenic factors [7]. Vascular endothelial growth factor (VEGF) and basic fibroblast growth factor (bFGF) are among the key initiators of neovascularization. They activate endothelial cells, stimulating their migration along concentration gradients, which promotes cell assembly, new vessel formation, and subsequent maturation [9]. VEGF acts by preventing endothelial cell apoptosis, a vital regulator for neovascularization during embryogenesis [10]. Similarly to VEGF, bFGF is a key factor in stimulating endothelial cell proliferation *in vitro* and promoting angiogenesis *in vivo* [11]. Studies also suggest that bFGF acts as an indirect angiogenic factor by modulating the expression of VEGF [11]. Another strategy to enhance vascularization in engineered tissues and promote their functionality is the use of bioreactors [12]. Specifically, perfusion and rotating bioreactors have been used to overcome mass transport limitations in culture, with perfusion bioreactors being particularly useful for the *in vitro* development of functional vascular structures. In addition, perfusion exposes cells to fluid shear stress, an important mechanical cue for maintaining endothelial integrity and function in vascularized tissues [13–15] Bioreactors are designed to mimic aspects of the *in vivo* environment by improving mass transport and, depending on the system, can provide mechanical, electrical, or perfusion-based stimulation to engineered tissues during *in vitro* culture [12].

Despite these advances, key research issues remain: (1) effectively enhancing *in vitro* vascularization within 3D

bioprinted cardiac constructs, and (2) supporting cardiomyocyte attachment, maturation, and functional behavior within the constructs. Addressing these challenges is essential for the development of functional and viable engineered cardiac tissues using 3D bioprinting technology.

To address these challenges, we aimed to bioprint human umbilical vein endothelial cell (HUVEC)-laden constructs with architectures that recapitulate the native alignment of cardiac myofibrils. Following endothelial network formation induced by VEGF, bFGF, and dynamic bioreactor conditioning, the constructs were subsequently seeded with cardiomyocytes to evaluate whether pre-vascularization enhances cardiac cell organization and coordinated contractile behavior.

Materials and methods

Cell culture

Human umbilical vein endothelial cells

HUVECs (ATCC 1730-CRL) were cultured in complete culture medium composed of DMEM (SH30243.01, HyClone, Cytiva) supplemented with 2% HAT (50×) (sodium hypoxanthine, aminopterin, and thymidine; 21060017, Gibco, ThermoFisher), 10% fetal bovine serum (FBS; Gibco, Invitrogen), and 1% antibiotic-antimycotic (100×) containing 10,000 U/mL penicillin, 10,000 µg/mL streptomycin, and 25 µg/mL Fungizone (15240062, Gibco, ThermoFisher). Cells were maintained at 37 °C in a humidified atmosphere containing 5% CO_2, and the culture medium was replaced every 2–3 days until they reached approximately 80% confluency. Before each bioprinting experiment, frozen HUVECs were thawed, expanded for several passages to obtain the required cell number, and harvested using trypsinization for bioink preparation. The cells were then resuspended in the bioink at a final density of 6×10^6 cells/mL. To ensure experimental consistency, HUVECs were used at the same passage number throughout the study.

H9c2 cells

H9c2 cells (ATCC CRL-1446) were cultured in DMEM supplemented with 10% fetal bovine serum (FBS) and 1% antibiotic-antimycotic (100×). Cells were maintained at 37 °C in a humidified atmosphere containing 5% CO_2, and the culture medium was replaced every 2–3 days until they reached approximately 80% confluency. Cells were maintained below passage 15 throughout the study. Prior to seeding onto the constructs, the cells were harvested by trypsinization and seeded at a density of 20×10^4 cells per construct.

Neonatal rat ventricular myocytes

Two-day-old neonatal Sprague-Dawley rat pups from Charles River were euthanized by decapitation, and their hearts were collected in PBS containing 5 mM glucose (Sigma G7021) for experimental purposes. All procedures followed the guidelines set by the Canadian Council of Animal Care and were approved by the Animal Research Ethics Board at the University of Saskatchewan (AUP #20220090). Following removing the atria and large vessels, the ventricles were enzymatically digested using a lysis buffer solution containing 20 mM HEPES-NaOH (Cat. No. S5011, Sigma), 130 mM NaCl (Cat. No. S5886, Sigma), 3 mM KCl (Cat. No. P5405, Sigma), 1 mM NaH2PO4 (Cat. No. S5011, Sigma), 5 mM glucose, 15 mg/mL DNase I (Cat. No. 104159, Roche), collagenase Type II (Cat. No. 17101015, ThermoFisher), and pancreatin (Cat. No. P3292, Sigma). Enzymatic digestion was carried out in multiple rounds, with the tissue incubated in 10 mL of lysis buffer at 37 °C for 10 min. The supernatant from the first round was discarded, and 4–6 additional rounds were performed, during which the supernatant was collected in 5 mL of horse serum (Cat. No. 16050130, ThermoFisher). After complete digestion of the tissue, the cells were pelleted by centrifugation at 300 x g for 5 min at 4 °C. The cell pellet was then re-suspended in pre-warmed red blood cell lysis buffer (Sigma 11814389001) and incubated for 3 min at 37 °C. Subsequently, 20 mL of pre-plating medium (DMEM/F-12 (Cat. No. 11320033, ThermoFisher) supplemented with 10% FBS (Cat. No. A5256701, ThermoFisher) and 1% Penicillin-Streptomycin (Cat. No. 15140122, ThermoFisher) was added, and the mixture was centrifuged again at 300 x g for 5 min at 4 °C. The cell pellet was re-suspended in the pre-plating medium and plated on uncoated cell culture dishes for 2 h to eliminate fibroblasts and endothelial cells. The non-adherent cells were collected, filtered through a 70µm mesh, centrifuged at 200 x g for 5 min at 4 °C, and re-suspended in culture medium (DMEM/F-12, 10% FBS, 1% Penicillin-Streptomycin, 5% horse serum (Cat. No. 16050130, ThermoFisher), 3 mM Na-pyruvate (Cat. No. S8636, Sigma), 0.1 mM ascorbic acid (Cat. No. A4034, Sigma), 1:200 insulin/transferrin/Na-Selenite solution (Cat. No. 51300044, Invitrogen), 0.2% BSA (Cat. No. A7409, Sigma), and 20 µM ara-C (Cat. No. C1768, Sigma)). The NRVM cells were seeded at a density of 50×10^4 cells per construct. The medium was replaced the following day to remove dead cells. Freshly isolated NRVMs were used directly for all experiments without prior passaging or expansion.

Induced pluripotent stem cell derived cardiomyocytes

Human induced pluripotent stem cell (iPSC)-derived cardiomyocytes (Cat. No. CSC-C2847SC; Creative Bioarray, USA) were thawed according to the manufacturer's protocol and seeded onto the constructs at a density of 50×10^4 cells per construct using the SuperCult Human Cardiomyocytes Medium Kit (Cat. No. CM-7863M). The kit includes both plating medium, which was used on the day of thawing, and maintenance medium, which replaced the plating medium 1 day after seeding according to the manufacturer's instructions. The maintenance medium was subsequently changed every other day. Cells were used immediately after thawing and were not expanded or passaged prior to seeding.

Bioink preparation

Bioink was prepared from a combination of 3 wt% alginic acid sodium salt from brown algae (A2033, Sigma-Aldrich) and 1 wt% gelatin (G1890, Type A, gel strength ~300 g Bloom, Sigma-Aldrich), denoted as Alg3Gel1, encapsulating HUVECs at a density of 6×10^6

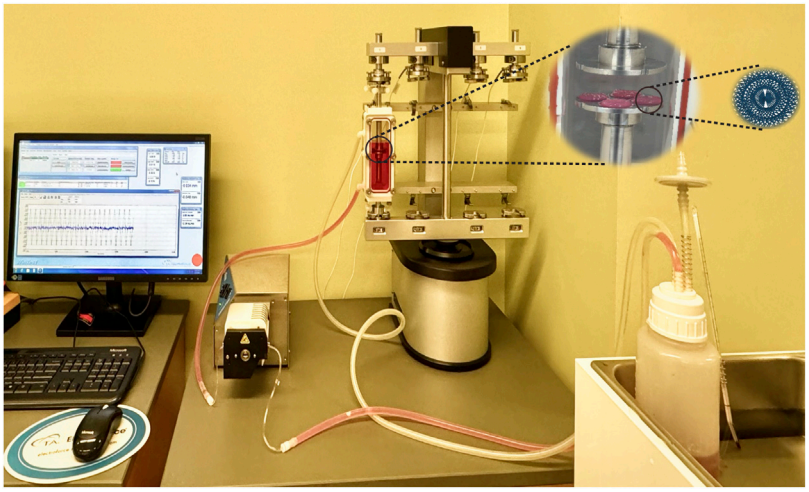


FIGURE 1
Bioreactor setup. The image shows the bioreactor chamber with circulating media controlled by a peristaltic pump. Four constructs are positioned between two plates. During operation, the constructs were subjected to a triangular compressive force at a frequency of 1 Hz.

cells/mL. The alginate/gelatin bioink (Alg3Gel1) used in this study has been previously optimized and comprehensively characterized, including its rheological behavior, mechanical properties, printability, and ability to support endothelial cell viability [16, 17]. To further enhance cell proliferation, 100 ng/mL of VEGF (PHC9391, Gibco, ThermoFisher) and 100 ng/mL of bFGF (PHG0369, Gibco, ThermoFisher) were incorporated into the bioink in the present study.

Bioprinting cardiac constructs

A 3D construct was designed with a circular shape (9 mm in diameter), an infill distance of 1.5 mm, and a strand diameter of 0.15 mm, as per our previous study [16]. The constructs were fabricated in 16 layers using a BioScaffolder 3.2 (Gesim, Germany) equipped with a 27G SmoothFlow Tapered Tip (inner diameter: 0.2 mm, EFD, Nordson). The printing head operated at a velocity of 4 mm/s with a printing pressure of 25 kPa, as optimized in our previous study [17]. The constructs were 3D bioprinted with a hierarchical structure, where each layer was rotated by +10° relative to the previous one. The first layer was oriented at −70°, and the last layer was oriented at +80°. The constructs were 3D bioprinted into 12-well plates that had been coated with 0.1% polyethyleneimine (PEI, M.W. 60,000, 50% w/w aqueous, Thermo Scientific) and incubated overnight at 37 °C. Immediately before printing, the 0.1% PEI solution was replaced with a prewarmed (37 °C) printing solution composed of 50 mM calcium chloride (CaCl2) in 0.1% PEI. The tissue constructs were then 3D bioprinted into the wells filled with the printing solution and left in the solution for an additional 15-min post-printing to facilitate cross-linking. Following this, the constructs were washed three times with DMEM, and complete culture media prepared for HUVECs was added to each well. On the same day, the constructs were impregnated with collagen type I from rat tail (A1048301, Gibco, ThermoFisher), diluted to 1.5 mg/mL in DMEM, and transferred to a new plate.

Static and dynamic culture of 3D bioprinted constructs

The constructs were cultured in a humidified incubator at 37 °C with 5% CO_2. From the beginning of the study, the constructs were assigned to one of three experimental groups: (1) control (CTRL), maintained under static culture without growth factor (GF) supplementation or bioreactor conditioning; (2) growth factor-treated (GF), maintained under static culture and supplemented with VEGF and bFGF during the first 10 days of culture; and (3) growth factor plus bioreactor-conditioned (GF + BIO), supplemented with VEGF and bFGF during the first 10 days of culture and subsequently subjected to dynamic bioreactor conditioning. To allow initial cell attachment and proliferation, all constructs were maintained under static conditions for the first 10 days following 3D bioprinting. On Day 10, when endothelial network formation was initiated, the GF + BIO constructs were transferred to the bioreactor (ElectroForce BioDynamic 5200, TA Instruments, Eden Prairie, MN, USA) and subjected to compressive loading and perfusion to partially simulate the cardiac environment. Dynamic conditioning was performed for one hour per day over three consecutive days (Figure 1), while CTRL and GF groups remained under static culture for the remainder of the experiment.

The device platens allowed for the simultaneous placement of four separate constructs. The constructs were subjected to a triangular compressive force at a frequency of 1 Hz, mimicking the physiological frequency experienced by the heart muscles [18]. The constructs were subjected to media perfusion at a flow rate of 5 mL/min using a peristaltic pump [19], with the temperature maintained at 37 °C using a water bath. The constructs were compressed with 3% strain to remain within their elastic region, as determined in our previous study [17]. After one hour of dynamic culture, the samples were returned to their plates and maintained in a static incubator.

Cell viability assay

To assess the viability and endothelialization of the endothelial cells across the three groups, the viability and morphology of the cells were evaluated by labelling live cells with green fluorescent using 1 μg/mL calcein AM (AnaSpec, Fremont) and dead cells with red fluorescent using 10 μg/mL of propidium iodide (PI, AnaSpec, Fremont) at the end of the 21-day incubation period. The constructs were subsequently imaged using a Leica TCS SPE II confocal microscope.

Cardiomyocyte seeding

To establish a pre-vascularized microenvironment prior to cardiomyocyte introduction, HUVEC-laden constructs were first cultured to allow endothelial network formation before cardiomyocyte seeding. H9c2 cells were used for preliminary studies, whereas NRVMs and iPSC-CMs were used to evaluate the performance of the engineered constructs. Cardiomyocytes were seeded after a total culture period of 15–16 days following 3D bioprinting and maintained under standard culture conditions until the designated experimental endpoint.

Immunofluorescence staining

For histological analyses, at the end of the 21 days, the tissue constructs were fixed in 4% paraformaldehyde (PFA) at 4 °C for one hour. Following fixation, the tissues were processed using either Cryosectioning or whole-mount staining.

Cryosectioning and staining

Fixed samples were sequentially incubated in a 15% and 30% sucrose solution (1 h each, 4 °C), embedded in frozen section compound (Cat. No. 95057–838), and snap-frozen in 2-methylbutane (106056, Millipore Sigma) on dry ice. Samples were stored at −80 °C until sectioning. Cryosections (20 μm) were obtained using an Avantik Biogroup cryostat (Avantik Biogroup LLC QS 11) at −25 °C on pre-coated glass slides (coated with 0.5% gelatin dissolved in 0.1% polyethyleneimine solution, incubated at 37 °C overnight).

Sections were dried at room temperature and subjected to blocking/permeabilization (1 h; 0.1% Triton X-100, bovine serum albumin, donkey serum in Hanks' Balanced Salt Solution (HBSS)), followed by overnight incubation at 4 °C with primary antibodies, including rabbit recombinant monoclonal CD31 antibody (1:500, ab76533, Abcam), cardiac troponin T monoclonal antibody (cTnT; MA5-12960, Invitrogen), connexin 43 monoclonal antibody (Cx43; 1:500, 13–8300, Invitrogen), and sarcomeric α-actinin (ACTN2) monoclonal antibody (A7732, Sigma). After washing the slides with HBSS, sections were incubated with appropriate Alexa Fluor secondary antibodies, including Alexa Fluor™ 488 (1:200, donkey anti-rabbit IgG (H + L), A-21206, Invitrogen), Alexa Fluor™ 647 (1:200, donkey anti-mouse IgG (H + L), A-31573, Invitrogen), Alexa Fluor™ 555 (1:200, donkey anti-mouse IgG (H + L), A-31570, Invitrogen), and 4′,6-diamidino-2-phenylindole (DAPI) for 2 h at room temperature protected from light. Sections were washed 5 times with HBSS, and they were mounted using ProLong™ Gold Antifade Reagent (Cat. #P36930) and imaged using a Nikon CSU-X1 confocal microscope.

Whole-mount staining

For whole-mount staining, constructs were incubated in blocking/permeabilization solution for one hour, followed by overnight incubation at 4 °C with the primary antibodies at the same dilutions specified in Section *Cryosectioning and staining*. Following washing, constructs were incubated with the corresponding Alexa Fluor secondary antibodies at 1:200 dilution for three hours at room temperature with gentle agitation. Samples were washed and imaged using a Nikon CSU-X1 confocal microscope.

Experimental design considerations

Due to the limited resources of primary cardiac cells (NRVMs and iPSC-CMs) and bioreactor capacity constraints (four constructs per run), constructs were allocated to either whole-mount immunofluorescence or cryosectioning. Whole-mount imaging preserved 3D architecture, whereases cryosectioning enabled complementary structural analysis.

Image processing

Z-stack images were acquired and converted to maximum intensity projections. Images were processed in ImageJ by conversion to 8-bit, contrast enhancement, and saturation adjustment (0.35). Thresholding was performed using the Huang method to generate binary masks, followed by particle analysis (minimum size = 100).

For cardiomyocyte analysis, cTnT-positive area was quantified from representative whole-mount images using the same image processing pipeline. The total cTnT-positive area was normalized to the field of view and expressed as percentage coverage. Due to the limited number of biological replicates and reliance on representative imaging fields, this analysis is reported as semi-quantitative.

Endothelial marker quantification

CD31 expression was quantified in cryosectioned vascularized constructs (n = 4) not seeded with cardiomyocytes. The sectioned samples were used to visualize the endothelial structures within the construct. CD31-positive area was quantified and normalized to DAPI-positive area to account for cell density.

Calcium imaging

The constructs were incubated with 5 μM Fluo-8 (Cat. No. ab142773, Abcam) in NRVM complete medium for 1.5 h at 37 °C. After incubation, they were washed twice with fresh NRVM complete medium for 5 min each at 37 °C. Calcium transients in NRVM-seeded constructs were imaged using a Nikon CSU-X1 confocal microscope equipped with 10× and 20× objectives on a heated stage maintained at 37 °C. Videos were recorded for 15 s, and the imaging data were analyzed using OriginLab and visualized with GraphPad Prism. For calcium transient analysis, three regions of

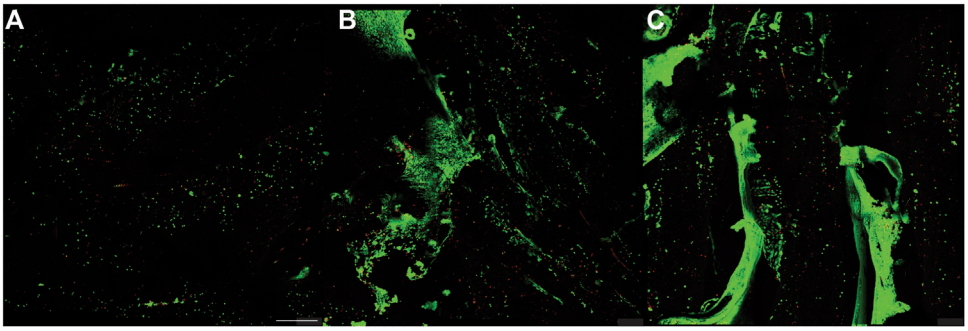


FIGURE 2
Live/dead staining images of bioprinted constructs, **(A)** CTRL group: constructs incubated only under static conditions. **(B)** GF group: constructs incubated only under static conditions supplemented with GFs, during the first 10 days of static incubation. **(C)** GF + BIO group: constructs incubated under static and dynamic conditions supplemented with GFs during the first 10 days of static incubation. The scale is 500 μm.

interest (ROIs) were randomly selected at day 17 (1 day after seeding the NRVMs). On day 21, the entire recorded frame was used for analysis. The same imaging and analysis protocol was applied to constructs seeded with iPSC-CMs. Calcium transients were quantified as the fractional change in fluorescence intensity (F) relative to baseline fluorescence (F_0), expressed as F/F_0 [20].

Results

Dynamic incubation enhances endothelial network formation in HUVEC-laden constructs

Live/dead assay was used to qualitatively assess cell viability and endothelial network formation across the experimental groups (Figure 2). In CTRL group (Figure 2A), where the 3D printed constructs were neither treated with GFs nor subjected to the bioreactor conditioning, limited cell viability was observed. Cells predominantly exhibited a spherical morphology, and no evidence of endothelial organization was detected; these are hereafter referred to as non-vascularized constructs.

In GF group (Figure 2B), where constructs were treated with GFs but not exposed to bioreactor conditions increased cell viability was noted compared to CTRL group, with cells displaying random distribution and early signs of endothelial organization, suggesting partial initiation of vascular network formation. In contrast, GF + BIO group (Figure 2C), which received both GF treatment and bioreactor conditioning, cell viability was markedly enhanced and the formation of continuous, interconnected endothelial networks throughout the constructs was observed. These constructs are hereafter referred to as vascularized constructs.

Vascularized constructs exhibit organized endothelial networks

Following the identification of GF + BIO group as the optimal condition for endothelial network formation (hereafter referred to as vascularized constructs), H9C2 cells were seeded onto the constructs at days 15–16 and cultured until day 21.

Immunofluorescence analysis (Figure 3) demonstrated the expression of ACTN2 in H9C2 cells (Figure 3A), CD31 in HUVECs (Figure 3B), and Cx43 in HUVECs (Figure 3C). CD31 and Cx43 expression was prominently localized along continuous, vessel-like structures, indicating the presence of organized and interconnected endothelial networks within the constructs.

ACTN2 expression was observed throughout the constructs, confirming the presence of cardiomyocytes; however, no distinct sarcomeric organization was evident, suggesting that the cardiac cells remained in an immature state at this stage.

To assess the consistency of endothelial cell distribution within the vascularized constructs, CD31 fluorescence was normalized to DAPI fluorescence. The resulting CD31/DAPI ratio was 0.98 ± 0.03 (n = 4), indicating reproducible endothelial cell distribution among the vascularized constructs and supporting the representative CD31-positive networks shown in (Figure 4).

Cardiomyocyte integration depends on vascularization (NRVMs)

To further assess cardiomyocyte integration within the bioprinted constructs in a pre-clinically relevant model, NRVMs were used in place of H9c2 cells. NRVMs were seeded onto the constructs at day 16, and samples were fixed at day 21 with 4% PFA, followed by whole-mount immunofluorescence staining. CD31 was used to label HUVECs while cTnT was used to identify NRVMs.

To evaluate the influence of vascularization on NRVM behaviour, cells were seeded onto both non-vascularized and vascularized constructs. As shown in Figures 5A,B, NRVMs seeded on non-vascularized constructs expressed cTnT and exhibited a typical morphology, with no clear association with endothelial structures, consistent with the limited presence of endothelial cells observed in this group.

In contrast, NRVMs seeded on vascularized constructs (Figures 5C,D) not only expressed cTnT but also preferentially adhered to and aligned with CD31-positive endothelial networks, showing enhanced structural integration with the preformed vascular-like architecture.

Semi-quantitative analysis of representative fields (Figure 5E) further supported these observations, showing greater cTnT-

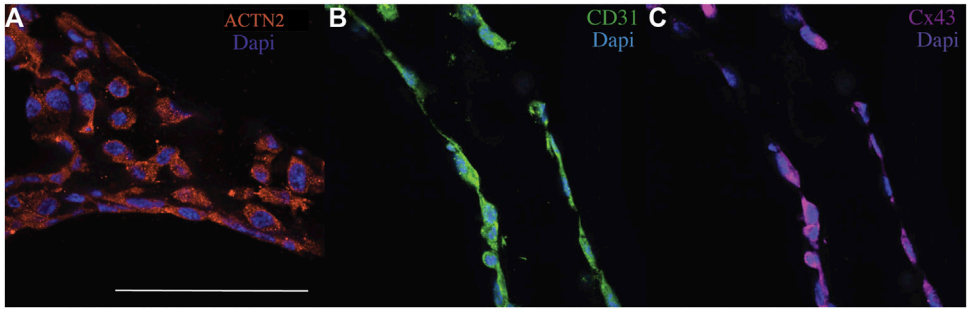


FIGURE 3
Immunofluorescence images from embedded cryosection staining of 3D bioprinted constructs (GF + BIO group) seeded with H9c2 **(A)** H9c2 cells seeded onto the constructs expressing ACTN2, **(B)** HUVECs forming tubular structures and expressing CD31, **(C)** HUVECs expressing connexin 43 (Cx43). The scale bar is 100 mm.

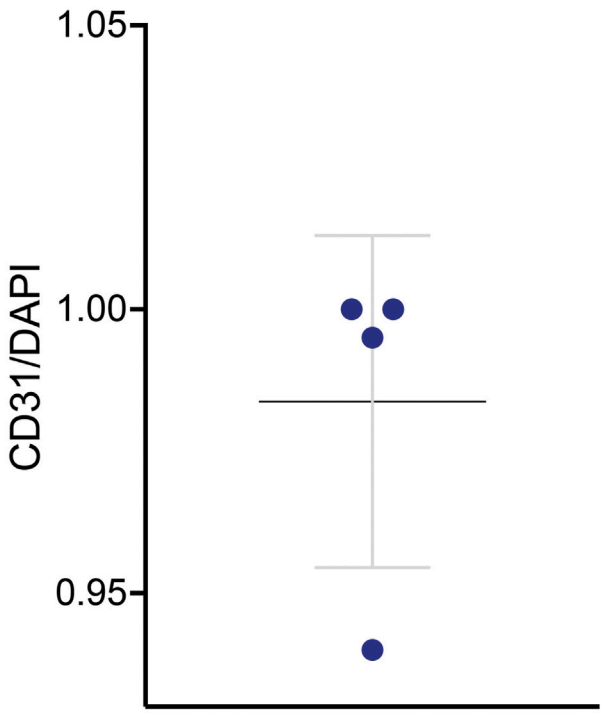


FIGURE 4
Quantification of CD31-positive area normalized to DAPI in vascularized constructs. Each dot represents one independent sample (n = 4). Data are presented as mean ± SD.

positive coverage and enhanced spatial continuity of NRVMs in vascularized constructs (43.6%) relative to non-vascularized constructs (31.5%).

iPSC-CMs show enhanced structural organization in vascularized constructs

To further mimic the native cardiac tissue environment, iPSC-CMs were seeded onto the constructs at day 16 as the final stage of the study, as a clinically relevant model of CTE.

As shown in Figure 6, iPSC-CMs expressed cTnT on both vascularized and non-vascularized constructs. In the non-vascularized constructs (Figures 6A,B), iPSC-CMs formed rounded and compact clusters with limited spreading, indicative of immature structural organization. Although cTnT-positive area was observed, the cells displayed limited spatial organization. The absence of CD31 staining confirmed that these constructs lacked endothelial network formation.

In contrast, iPSC-CMs seeded on vascularized constructs (Figures 6C,D) exhibited elongated, aligned, and continuous cTnT-positive area that were spatially associated with CD31-positive endothelial networks, indicating enhanced structural organization and cardiomyocyte–endothelial integration. Semi-quantitative analysis of representative fields (Figure 6E) further supported these observations, showing greater cTnT-positive area and enhanced spatial continuity of iPSC-derived cardiomyocytes in vascularized constructs (52.6%) relative to non-vascularized constructs (23.4%).

NRVMs and iPSC-CMs seeded on vascularized 3D bioprinted constructs exhibit enhanced contractile behaviour

Calcium transient imaging was performed independently on vascularized and non-vascularized constructs seeded with either NRVMs or iPSC-CMs to evaluate cardiomyocyte function (Figure 7). For NRVM-seeded constructs, imaging was conducted at day 17 (1 day after seeding) and day 21, while iPSC-CM–seeded constructs were assessed at day 21.

At day 17, NRVMs seeded on non-vascularized constructs showed a rounded and isolated morphology, and exhibited spontaneous beating (Figures 7a1,b1; Supplementary Material 1). In contrast, NRVMs seeded on vascularized constructs displayed more elongated and aligned cell morphology, along with synchronized contractions and more rhythmic activity (Figures 7a2,b2; Supplementary Material 2).

By day 21, NRVMs in both groups maintained contractile activity. However, cells on non-vascularized constructs exhibited irregular and arrhythmic contractions despite increased elongation compared to day 17 (Figures 7a3,b3; Supplementary Material 3). In contrast, NRVMs on vascularized constructs retained coordinated

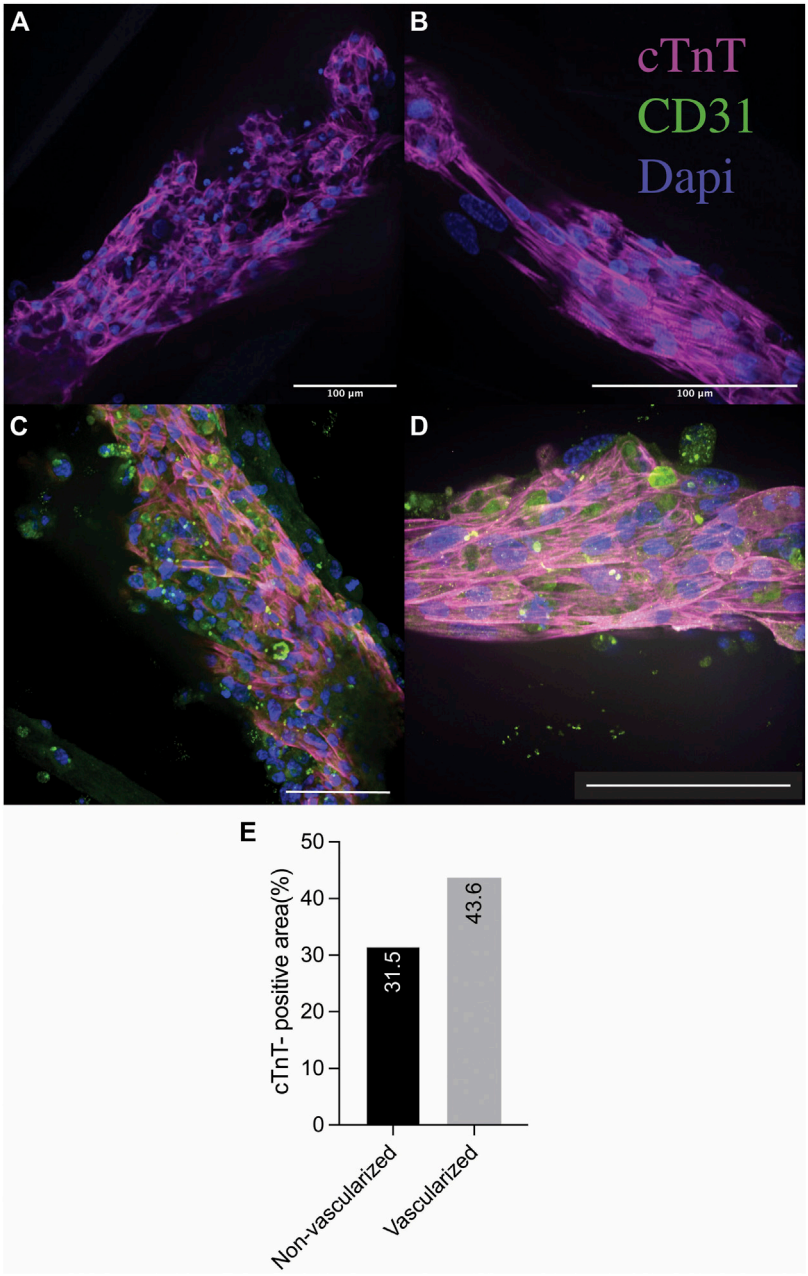


FIGURE 5
Structural organization of cardiomyocytes and endothelial networks in vascularized and non-vascularized 3D bioprinted constructs seeded with NRVMs. **(A,B)** NRVMs seeded onto non-vascularized control constructs expressing cTnT with two different magnifications. **(C,D)** NRVMs seeded onto vascularized constructs expressing cTnT, with HUVECs expressing CD31 with two different magnifications. **(E)** Semi-quantitative analysis of cTnT-positive area based on representative fields. Bars represent the mean of selected images from a single construct (technical replicates). Constructs were fixed and stained as whole-mount samples without embedding. Scale bar = 100 µm.

and synchronous beating, accompanied by the formation of a more interconnected cellular network (Figures 7a4,b4; Supplementary Material 4), although with a slightly reduced beating frequency.

To further evaluate the performance of the engineered constructs using a human cardiac cell model, iPSC-CMs were seeded onto both vascularized and non-vascularized constructs and assessed on day 21. In non-vascularized constructs, beating was observed in isolated clusters, requiring the analysis of multiple regions of interest (ROIs) (Figure 7a5; Supplementary Material 5). In contrast, iPSC-CMs on vascularized constructs formed elongated, aligned, and continuous networks that contracted synchronously across the field of view, making it impractical to define separate ROIs (Figure 7a6; Supplementary Material 6).

Although the spontaneous beating frequency of iPSC-CMs on vascularized constructs (Figure 7b6) was lower than that of non-vascularized constructs, the contractions were highly synchronized within a well-organized cellular network. In contrast, non-vascularized constructs (Figure 7b5) exhibited more frequent but

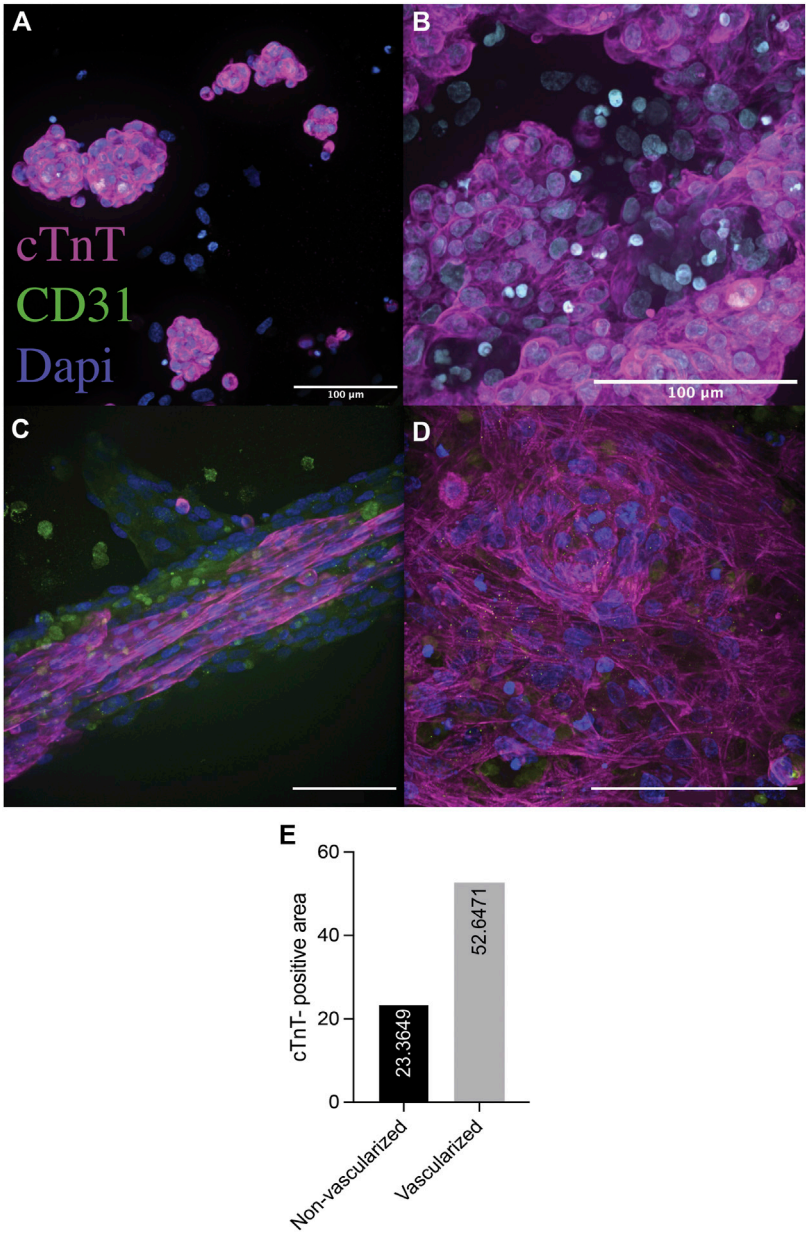


FIGURE 6
Structural organization of cardiomyocytes and endothelial networks in vascularized and non-vascularized 3D bioprinted constructs seeded with iPSC-CMs. **(A,B)** iPSC-CMs seeded onto non-vascularized control constructs expressing cTnT under two different magnifications. **(C,D)** iPSC-CMs seeded onto vascularized constructs expressing cTnT, with HUVECs expressing CD31 under two different magnifications. **(E)**Semi-quantitative analysis of cTnT-positive area based on representative fields. Bars represent the mean of selected images from a single construct (technical replicates). Constructs were fixed and stained as whole-mount samples without embedding. Scale bar = 100 µm.

unsynchronized contractions, with independent beating across isolated cell clusters. These observations suggest improved functional integration, as evidenced by the coordinated contractile behavior observed within the vascularized constructs.

Discussion

The aim of this study was to engineer a vascularized tissue construct capable of supporting cardiac cell function as a step toward engineering fully contractile, vascularized cardiac tissue. To achieve this, HUVECs were embedded in an alginate/gelatin matrix and 3D bioprinted in a hierarchical structure designed to mimic the orientation of cardiac myofibrils. Following bioprinting, the constructs were coated with type I collagen, given its essential role in vessel formation and stability, as well as its ability to act as a reservoir and modulator for proangiogenic factors such as VEGF and bFGF [21]. Our previous studies demonstrated that the hierarchical structure supports cell viability in both top-down [16] and bottom-up approaches [17]. Building upon that foundation, the current study integrated both strategies to advance the development of a

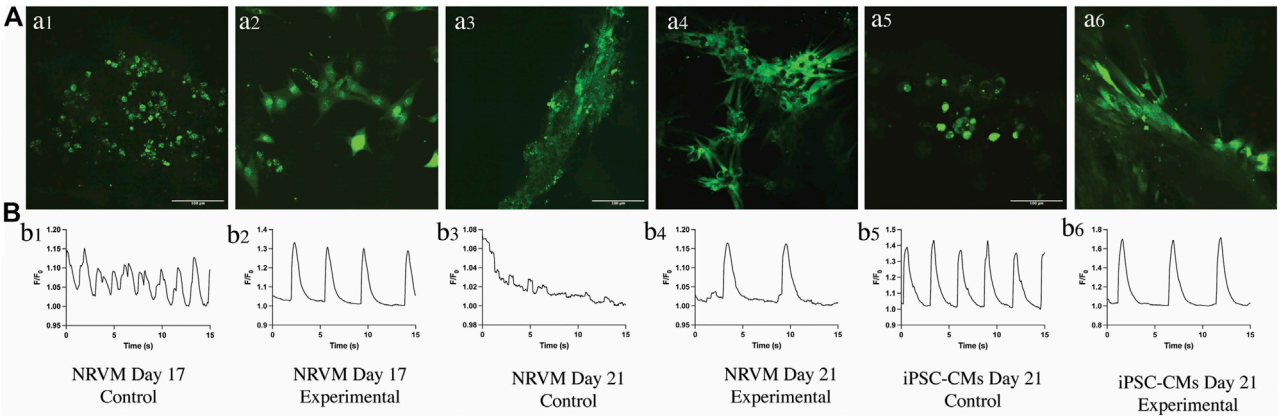


FIGURE 7
Calcium transient activity in NRVM- and iPSC-CM–seeded 3D bioprinted constructs at day 17 and day 21. **(A)** Representative fluorescence images showing Fluo-8–labeled calcium transients and **(B)** corresponding calcium transient traces for constructs seeded with neonatal rat ventricular myocytes (NRVMs) or human induced pluripotent stem cell–derived cardiomyocytes (iPSC-CMs). On day 17, three regions of interest (ROIs) were randomly selected for F/F0 analysis, whereas on day 21, the entire imaging field was analyzed as a single ROI. Scale bars: 100 μm.

vascularized cardiac patch capable of supporting endothelial and cardiac cell function.

To promote endothelial network formation within the engineered constructs, the experimental design followed a stepwise engineering approach, in which VEGF and bFGF supplementation was first used to support endothelial network formation, followed by dynamic bioreactor conditioning to determine whether perfusion and mechanical stimulation could further enhance endothelial organization. Live/dead assay results revealed that only the GF + BIO group developed organized and dense tubular vessels within the constructs (Figure 2), suggesting that the addition of dynamic bioreactor conditioning to growth factor-treated constructs enhanced endothelial network formation under the conditions evaluated in this study.

The combined use of VEGF and bFGF in promoting endothelial network formation has been widely reported in collagen-based systems [22, 23]. However, relatively few studies have combined these growth factors with perfusion-based culture to examine their use in promoting vascularization within engineered tissues [23]. One such study demonstrated enhanced cell migration under continuous flow with VEGF and bFGF supplementation [23]. In contrast to previous approaches, our study introduced a thick, multi-layered (16-layer) bioprinted construct with architecture mimicking myocardial alignment, combined with both perfusion and mechanical stimulation, thereby providing a more physiologically relevant microenvironment for endothelial organization.

Perfusion bioreactors enhance nutrients and oxygen transport within engineered tissues, enhancing mass transport throughout the scaffold [24]. In addition, mechanical stimulation has been shown to promote vascular alignment and network formation [25]. The combination of growth factor supplementation and dynamic bioreactor conditioning likely contributed to the enhanced endothelial network formation observed under the experimental conditions evaluated in this study.

Confocal imaging at day 21 confirmed that endothelial cells organized into interconnected, vessel-like networks (Figure 3B). Strong CD31 expression indicated the formation of intercellular junctions, while Cx43 expression suggested the development of gap junctions involved in intercellular communication (Figure 3C) [26]. Notably, Cx43 expression in endothelial cells has been associated with enhanced angiogenic potential, potentially through mechanisms independent of gap junction signaling [27].

Following the onset of endothelial network formation (approximately day 15), cardiomyocytes were seeded onto the constructs. H9c2 cells were initially used as a well-established *in vitro* cardiac cell model to evaluate the ability of the engineered constructs to support the attachment, viability and organization of cardiac cells. H9c2 cells adhered and expressed ACTN2 but did not exhibit contractile activity (Figure 3A). In contrast, NRVMs expressed cTnT and demonstrated robust contractility, aligning along preformed endothelial networks (Figure 5). These findings are consistent with previous studies showing enhanced integration of cardiomyocytes on pre-vascularized scaffolds [28]. Although NRVMs were also able to adhere and align on non-vascularized constructs, their alignment pattern and interaction with endothelial networks in vascularized constructs more closely recapitulate the native myocardial microenvironment.

Similarly, iPSC-CMs expressed cTnT in both conditions; however, their structural organization differed markedly. On non-vascularized constructs, cells remained rounded with limited alignment, whereas vascularized constructs supported the formation of elongated, aligned, and interconnected cellular networks (Figure 6).

Functional analysis further supported these structural observations. NRVMs on vascularized constructs exhibited more stable and synchronized contractile behavior compared to those on non-vascularized constructs (Figure 7). Similarly, iPSC-CMs on vascularized constructs demonstrated more coordinated and synchronized contractions, despite exhibiting a lower spontaneous beating frequency (Figure 7). These observations suggest improved functional integration, as evidenced by the coordinated contractile behavior observed within the vascularized

constructs. The improved synchronization and coordinated contractile behaviour observed in vascularized constructs seeded with NRVMs suggest that endothelial network formation may promote functional integration of cardiomyocytes within the constructs. Our findings are consistent with previous studies demonstrating that vascular cells can support the functional development of engineered cardiac tissues. For instance, a recent study has shown that the presence of vascular cells within human cardiac organoids enhances their maturation and force of contraction [29] likely by maintaining a minimal distance to provide oxygen and nutrients [30].

Calcium ions (Ca^{2+}) play a central role in excitation–contraction coupling, linking electrical activity to mechanical contraction in cardiomyocytes [31]. Accordingly, calcium transient imaging provides insightful information regarding excitation-contraction coupling. While cardiomyocytes on non-vascularized patches exhibited irregular and weak calcium transients, NRVMs on vascularized patches displayed more rhythmic and regular transients as early as 1 day after seeding, and this pattern remained consistent throughout the experimental period. This is supported by a previous study demonstrating that endothelial cells regulate the contractility of cardiac cells [32]. The study found that endothelial cells produce cardioactive factors in response to substances released during perfusion. These factors can affect both the strength and duration of contraction in adjacent cardiomyocytes [32]. These findings, together with previous reports, suggest that endothelial cells may contribute not only to nutrient and oxygen delivery but also to the regulation of cardiomyocytes contractile behaviour within engineered cardiac tissues.

While these findings demonstrate the potential of the developed constructs for cardiac tissue engineering applications, several limitations remain. The experimental duration was limited to 21 days, and longer culture periods may provide further insight into tissue maturation and hydrogel degradation. Furthermore, incorporation of quantitative analyses of calcium transient kinetics (e.g., rise time, decay time, and transient duration), together with force generation measurements, would provide a more comprehensive functional characterization of the engineered tissues. Future studies should explore optimization of cardiomyocyte seeding timing and bioreactor conditions to further enhance tissue development.

Conclusion

Cardiovascular diseases remain the leading cause of mortality worldwide, underscoring the urgent need for effective regenerative strategies, including CTE. Two major challenges in this field are the development of vascularized constructs and the support of functional cardiomyocyte behavior.

To address these challenges, this study employed 3D bioprinting to fabricate constructs that mimic the native orientation of cardiac myofibrils while incorporating endothelial cells to promote vascular-like network formation. Constructs were cultured under both static and dynamic conditions and subsequently seeded with cardiomyocytes.

Our results demonstrate that the incorporation of endothelial networks within bioprinted cardiac constructs enhances cell viability and may reduce the risk of necrotic core formation. Furthermore, the presence of endothelial networks improved the synchronization and organization of cardiomyocyte contractile behavior, highlighting the importance of endothelial–cardiomyocyte interactions in recapitulating native myocardial function.

Building upon our previous work in scaffold design and imaging-based characterization [33–39], this study integrates hierarchical architecture, endothelial network formation, and dynamic culture conditions to advance the development of functional cardiac tissue constructs. These findings provide a promising step toward more physiologically relevant engineered cardiac tissues and future regenerative applications.

Data availability statement

The original contributions presented in the study are included in the article/Supplementary Material, further inquiries can be directed to the corresponding authors.

Author contributions

FK: Conceptualization, investigation, experimental work, data analysis, writing – original draft, and review and editing. AK: NRVM isolation and culture, immunofluorescence and calcium transient data analysis, and review and editing. HA: Bioreactor optimization and review and editing. BE: Resources, provision of laboratory space and equipment, and review and editing. MC: Funding acquisition, resources for NRVM culture and calcium transient imaging, and review and editing. XC: Funding acquisition, supervision, conceptualization, provision of laboratory space and equipment, and review and editing. MK: Funding acquisition, supervision, conceptualization, provision of laboratory space and equipment, and review and editing. IB: Funding acquisition, supervision, conceptualization, provision of laboratory space and equipment, and review and editing. All authors contributed to the article and approved the submitted version.

Funding

The author(s) declared that financial support was received for this work and/or its publication. The authors acknowledge financial support for this work from the Natural Sciences and Engineering Research Council (NSERC) of Canada. This project received additional support through the Saskatchewan Research Chair in Clinical Stroke Research, awarded to MK by the Heart and Stroke Foundation, SHRF, and the University of Saskatchewan College of Medicine. This work also received financial support from the Knight Family Enhancement Chair in Neurological Surgery, awarded to MK. MC is supported by grants from the Canadian Institutes of Health Research (PJT-552376), he Natural Sciences and Engineering Research Council of Canada (RGPIN-2022-04756), the Canadian Foundation for Innovation, and a Heart and Stroke Foundation of Canada New Investigator award. AK is supported by funding from the College of Medicine, University of Saskatchewan and Canadian Institute of Health Research Canada Graduate Scholarship Masters

(CIHR CGS-M). FK was supported by the University of Saskatchewan Dean's Scholarship and the Biomedical Engineering Devolved Scholarship.

Conflict of interest

The author(s) declared that this work was conducted in the absence of any commercial or financial relationships that could be construed as a potential conflict of interest.

Generative AI statement

The author(s) declared that generative AI was used in the creation of this manuscript. F.K. used ChatGPT (OpenAI) to assist with language editing and manuscript preparation. All AI-assisted content was reviewed and approved by the authors, who take full responsibility for the final manuscript.

Any alternative text (alt text) provided alongside figures in this article has been generated by Frontiers with the support of artificial intelligence and reasonable efforts have been made to ensure accuracy, including review by the authors wherever possible. If you identify any issues, please contact us.

Supplementary material

The Supplementary Material for this article can be found online at: https://www.frontierspartnerships.org/articles/10.3389/jpps.2026.17204/full#supplementary-material

References

1. Selzman CH, Madden JL, Healy AH, McKellar SH, Koliopoulou A, Stehlik J, et al. Bridge to removal: a paradigm shift for left ventricular assist device therapy. *Ann Thorac Surg* (2015) 99:360–7. doi: 10.1016/j.athoracsur.2014.07.061

2. Kanwar MK, Selzman CH, Ton V-K, Miera O, Cornwell IIIWK, Antaki J, et al. Clinical myocardial recovery in advanced heart failure with long term left ventricular assist device support. *J Heart Lung Transpl* (2022) 41:1324–34. doi: 10.1016/j.healun.2022.05.015

3. Lu T-Y, Xiang Y, Tang M, Chen S. 3D printing approaches to engineer cardiac tissue. *Curr Cardiol Rep* (2023) 25:505–14. doi: 10.1007/s11886-023-01881-y

4. Hwang DG, Choi H, Yong U, Kim D, Kang W, Park S, et al. Bioprinting-assisted tissue assembly for structural and functional modulation of engineered heart tissue mimicking left ventricular myocardial fiber orientation. *Adv Mater* (2024) 36:2400364. doi: 10.1002/adma.202400364

5. Wong J, Kuhl E. Generating fibre orientation maps in human heart models using poisson interpolation. *Comput Methods Biomech Biomed Engin* (2014) 17:1217–26. doi: 10.1080/10255842.2012.739167

6. Bliley JM, Stang MA, Behre A, Feinberg AW. Advances in 3D bioprinted cardiac tissue using stem cell-derived cardiomyocytes. *Stem Cells Transl. Med.* (2024) 13:425–35. doi: 10.1016/j.yjmcc.2022.04.017

7. Cho S, Discher DE, Leong KW, Vunjak-Novakovic G, Wu JC. Challenges and opportunities for the next generation of cardiovascular tissue engineering. *Nat Methods* (2022) 19:1064–71. doi: 10.1038/s41592-022-01591-3

8. Williams MAC, Mair DB, Lee W, Lee E, Kim D-H. Engineering three-dimensional vascularized cardiac tissues. *Tissue Eng B Rev* (2022) 28:336–50. doi: 10.1089/ten.teb.2020.0343

9. Novosel EC, Kleinhans C, Kluger PJ. Vascularization is the key challenge in tissue engineering. *Adv Drug Deliv Rev* (2011) 63:300–11. doi: 10.1016/j.addr.2011.03.004

10. Poldervaart MT, Gremmels H, van Deventer K, Fledderus JO, Öner FC, Verhaar MC, et al. Prolonged presence of VEGF promotes vascularization in 3D bioprinted scaffolds with defined architecture. *J Control Release* (2014) 184:58–66. doi: 10.1016/j.jconrel.2014.04.007

11. Stavri GT, Zachary IC, Baskerville PA, Martin JF, Erusalimsky JD Basic fibroblast growth factor upregulates the expression of vascular endothelial growth factor in vascular smooth muscle cells. *Synergistic interaction with hypoxia* (1995) 92 11–4. doi: 10.1161/01.CIR.92.1.11

12. Paez-Mayorga J, Hernández-Vargas G, Ruiz-Esparza GU, Iqbal HMN, Wang X, Zhang YS, et al. Bioreactors for cardiac tissue engineering. *Adv Healthc Mater* (2019) 8:1701504. doi: 10.1002/adhm.201701504

13. Lim KT, Cho CS, Choung YH, Kim JH, Son HM, Woo HS, et al. Novel perfusion bioreactor systems for tissue engineering. *Regen Med* (2009) 6:207–18.

14. Nwokoye PN, Abilez OJ. Blood vessels in a dish: the evolution, challenges, and potential of vascularized tissues and organoids. *Front Cardiovasc Med* (2024) 11:1336910. doi: 10.3389/fcvm.2024.1336910

15. Lovett M, Lee K, Edwards A, Kaplan DL. Vascularization strategies for tissue engineering. *Tissue Eng. Part B Rev* (2009) 15(3):353–370. doi: 10.1089/ten.teb.2009.0085

16. Ketabat F, Maris T, Duan X, Yazdanpanah Z, Kelly ME, Badea I, et al. Optimization of 3D printing and *in vitro* characterization of alginate/gelatin lattice and angular scaffolds for potential cardiac tissue engineering. *Front Bioeng Biotechnol* (2023) 11:1161804.

17. Ketabat F, Gharraei R, Guinle A, Sylvain NJ, Kelly ME, Badea I, et al. Bioprinting and *in vitro* characterization of alginate-gelatin constructs incorporating human umbilical vein endothelial cells for potential cardiac tissue engineering. *Int J Bioprint* (2025). 11(5):385–407. doi: 10.3389/fbioe.2023.1161804

18. Wang B, Wang G, To F, Butler JR, Claude A, McLaughlin RM, et al. Myocardial scaffold-based cardiac tissue engineering: application of coordinated mechanical and electrical stimulations. *Langmuir* (2013) 29:11109–17. doi: 10.1021/la401702w

19. Lee EJ, Niklason LE. A novel flow bioreactor for *in vitro* microvascularization. *Tissue Eng C Methods* (2010) 16:1191–200. doi: 10.1089/ten.tec.2009.0652

20. Alegret N, Dominguez-Alfaro A, Mecerreyes D, Prato M, Mestroni L, Peña B. Neonatal rat ventricular myocytes interfacing conductive polymers and carbon nanotubes. *Cell Biol. Toxicol.* (2023) 39:1627–39. doi: 10.1007/s10565-022-09753-x

21. Hwang J, Kiick KL, Sullivan MO. VEGF-encoding, gene-activated collagen-based matrices promote blood vessel formation and improved wound repair. *ACS Appl Mater Inter* (2023) 15:16434–47. doi: 10.1021/acsami.2c23022

22. Pepper MS, Ferrara N, Orci L, Montesano R. Potent synergism between vascular endothelial growth factor and basic fibroblast growth factor in the induction of angiogenesis *in vitro*. *Biochem Biophys Res Commun* (1992) 189:824–31. doi: 10.1016/0006-291X(92)92277-5

23. Sakaguchi K, Shimizu T, Horaguchi S, Sekine H, Yamato M, Umezu M, et al. *In vitro* engineering of vascularized tissue surrogates. *Sci Rep* (2013) 3:1316. doi: 10.1038/srep01316

24. Zohar B, Blinder Y, Epshtein M, Szklanny AA, Kaplan B, Korin N, et al. Multi-flow channel bioreactor enables real-time monitoring of cellular dynamics in 3D engineered tissue. *Commun Biol* (2019) 2:158. doi: 10.1038/s42003-019-0400-z

25. Wang Y, Liu M, Zhang W, Liu H, Jin F, Mao S, et al. Mechanical strategies to promote vascularization for tissue engineering and regenerative medicine. *Burns Trauma* (2024) 12:tkae039. doi: 10.1093/burnst/tkae039

26. Meng J, Xiao B, Wu F, Sun L, Li B, Guo W, et al. Co-axial fibrous scaffolds integrating with carbon fiber promote cardiac tissue regeneration post myocardial infarction. *Mater Today Bio* (2022) 16:100415. doi: 10.1016/j.mtbio.2022.100415

27. Koepple C, Zhou Z, Huber L, Schulte M, Schmidt K, Gloe T, et al. Expression of Connexin43 stimulates endothelial angiogenesis independently of gap junctional communication *in vitro*. *Int J Mol Sci* (2021) 22:7400. doi: 10.3390/ijms22147400

28. Zhang YS, Arneri A, Bersini S, Shin S-R, Zhu K, Goli-Malekabadi Z, et al. Bioprinting 3D microfibrous scaffolds for engineering endothelialized myocardium and heart-on-a-chip. *Biomaterials* (2016) 110:45–59. doi: 10.1016/j.biomaterials.2016.09.003

29. Voges HK, Foster SR, Reynolds L, Mills RJ, Porrello ER, Quaife-Ryan GA, et al. Vascular cells improve functionality of human cardiac organoids. *Cell Rep* (2023) 42:112322. doi: 10.1016/j.celrep.2023.112322

30. Sekine H, Shimizu T, Hobo K, Sekiya S, Yang J, Yamato M, et al. Endothelial cell coculture within tissue-engineered cardiomyocyte sheets enhances neovascularization and improves cardiac function of ischemic hearts. *Circulation* (2008) 118:S145–52. doi: 10.1161/CIRCULATIONAHA.107.757286

31. Fearnley CJ, Roderick HL, Bootman MD Calcium signaling in cardiac myocytes. *Cold Spring Harb. Perspect. Biol* (2011) 3 a004242. doi: 10.1101/cshperspect.a004242

32. Ramaciotti C, Sharkey A, McClellan G, Winegrad S. Endothelial cells regulate cardiac contractility. *Proc Natl Acad Sci USA* (1992) 89:4033–6. doi: 10.1073/pnas.89.9.4033

33. Ketabat F, Alcorn J, Kelly ME, Badea I, Chen X. Cardiac tissue engineering: a journey from scaffold fabrication to *in vitro* characterization. *Small Sci* (2024) 4:2400079. doi: 10.1002/smsc.202400079

34. Izadifar M, Chapman D, Babyn P, Chen X, Kelly ME. UV-assisted 3D bioprinting of nanoreinforced hybrid cardiac patch for myocardial tissue engineering *Tissue Eng. Part C methods*. *Tissue Eng Part C Methods* (2018) 24:74–88. doi: 10.1089/ten.tec.2017.0346

35. Izadifar M, Babyn P, Kelly ME, Chapman D, Chen X. Bioprinting pattern-dependent electrical/mechanical behavior of cardiac alginate implants: characterization and *ex vivo* phase-contrast microtomography assessment. *Tissue Eng Part C Methods* (2017) 23:548–64. doi: 10.1089/ten.tec.2017.0222

36. Izadifar M, Babyn P, Chapman D, Kelly ME, Chen X. Potential of propagation-based synchrotron X-ray phase-contrast computed tomography for cardiac tissue engineering. *J Synchrotron Radiat* (2017) 24:842–53. doi: 10.1107/S1600577517006208

37. Izadifar M, Kelly ME, Chen X. Regulation of sequential release of growth factors using bilayer polymeric nanoparticles for cardiac tissue engineering. *Nanomedicine* (2016) 11:3237–59. doi: 10.2217/nnm-2016-0220

38. Bai X, Fang R, Zhang S, Shi X, Wang Z, Chen X, et al. Self-cross-linkable hydrogels composed of partially oxidized alginate and gelatin for myocardial infarction repair. *J. Bioact. Compat. Polym.* (2013) 28(2):126–140. doi: 10.1177/0883911512473230

39. Bai XP, Zheng HX, Fang R, Wang TR, Hou XL, Li Y, et al. Fabrication of engineered heart tissue grafts from alginate/collagen barium composite microbeads. *Biomed Mater* (2011) 6:45002. doi: 10.1088/1748-6041/6/4/045002